Causal interactions between fronto-parietal central executive and default-mode networks in humans

Ashley C. Chen[a,b], Desmond J. Oathes[a,b], Catie Chang[c,d,e], Travis Bradley[a], Zheng-Wei Zhou[f], Leanne M. Williams[a,b], Gary H. Glover[c,d], Karl Deisseroth[a,g,h,1], and Amit Etkin[a,b,1]

Departments of [a]Psychiatry and Behavioral Sciences, [c]Electrical Engineering, [d]Radiology, and [g]Bioengineering, Stanford University, Stanford, CA 94305; [b]Sierra-Pacific Mental Illness Research, Education, and Clinical Center, Veterans Affairs Palo Alto Health Care System, Palo Alto, CA 94304; [e]Advanced MRI Section, Laboratory of Functional and Molecular Imaging, National Institute of Neurological Disorders and Stroke, National Institutes of Health, Bethesda, MD 20892; [f]Department of Biomedical Engineering, Tsinghua University, Beijing 100084, China; and [h]Howard Hughes Medical Institute, Stanford University, Stanford, CA 94305

Edited by Marcus E. Raichle, Washington University in St. Louis, St. Louis, MO, and approved October 24, 2013 (received for review June 25, 2013)

Information processing during human cognitive and emotional operations is thought to involve the dynamic interplay of several large-scale neural networks, including the fronto-parietal central executive network (CEN), cingulo-opercular salience network (SN), and the medial prefrontal-medial parietal default mode networks (DMN). It has been theorized that there is a causal neural mechanism by which the CEN/SN negatively regulate the DMN. Support for this idea has come from correlational neuroimaging studies; however, direct evidence for this neural mechanism is lacking. Here we undertook a direct test of this mechanism by combining transcranial magnetic stimulation (TMS) with functional MRI to causally excite or inhibit TMS-accessible prefrontal nodes within the CEN or SN and determine consequent effects on the DMN. Single-pulse excitatory stimulations delivered to only the CEN node induced negative DMN connectivity with the CEN and SN, consistent with the CEN/SN's hypothesized negative regulation of the DMN. Conversely, low-frequency inhibitory repetitive TMS to the CEN node resulted in a shift of DMN signal from its normally low-frequency range to a higher frequency, suggesting disinhibition of DMN activity. Moreover, the CEN node exhibited this causal regulatory relationship primarily with the medial prefrontal portion of the DMN. These findings significantly advance our understanding of the causal mechanisms by which major brain networks normally coordinate information processing. Given that poorly regulated information processing is a hallmark of most neuropsychiatric disorders, these findings provide a foundation for ways to study network dysregulation and develop brain stimulation treatments for these disorders.

task positive network | task negative network | fMRI | neuromodulation

Extensive neuroimaging work has described a set of large-scale, intrinsically organized networks in the human brain, as well as those of other mammals, which are thought to underlie a broad range of functions, from basic sensory and motor capacities to cognition and higher-level functions (1–4). Three networks in particular have been the focus of work related to these higher-level functions (5): the fronto-parietal central executive network (CEN), the cingulo-opercular salience network (SN), and the medial prefrontal-medial parietal default mode network (DMN). These networks are thought to interact and together control attention, working memory, decision making, and other higher-level cognitive operations (6–8).

Findings to date, however, emphasize the need for a direct test of the proposed causal relationship between these networks. On the basis of observations in resting-state functional MRI (rs-fMRI) scans in humans of time-locked negative CEN/DMN and SN/DMN connectivity (9–11), as well as mathematical modeling of temporal relationships between these networks (12), it has been argued that the CEN and/or SN negatively regulate activity in the DMN. However, because a similar pattern of connectivity can be spuriously introduced during data processing, interpretation of this negative connectivity as reflecting a genuine mechanistic relationship has been questioned (11). Thus, unknown is whether the DMN is indeed under causal control, and if so, which nodes within the CEN or SN can achieve this control. Answering these questions would inform the specific mechanisms by which opposing network dynamics may drive cognition (13) and thus extend beyond the view offered by current theoretical and clinical models of brain organization (14). Inferring causality from neuroimaging data, however, requires that normally correlative neuroimaging methods be combined with a direct external manipulation of neural activity in one or more of these networks.

We achieved a direct test of causality by combining two non-invasive techniques: transcranial magnetic brain stimulation (TMS) was used to directly excite or inhibit the CEN and SN, whereas concurrent neuroimaging with fMRI was used to determine the causal downstream consequences of TMS on the DMN (15). Concurrent TMS/fMRI builds on conventional neuroimaging approaches, wherein brain activation *correlates* are found across tasks or groups, by allowing direct excitation or inhibition of targeted brain regions and their interconnected distal network partners (15–17). Experimental manipulation of brain activity thereby provides information about causality not possible with correlative neuroimaging alone, and it can be achieved with high reliability and precision, with induced fMRI responses resembling voluntarily evoked brain activity (18). Application of this technology to a systems-level understanding of causal interactions among the CEN,

Significance

Three large-scale neural networks are thought to play important roles in cognitive and emotional information processing in humans. It has been theorized that the "central executive" and "salience" networks achieve this by regulating the "default mode" network. Support for this idea comes from correlational neuroimaging studies; however, direct evidence for this neural mechanism is lacking. We tested this hypothesized mechanism by exciting or inhibiting nodes within the central executive and salience networks using noninvasive brain stimulation and observed the results using simultaneous brain imaging. We found that the default mode network is under inhibitory control specifically from a node in the central executive network, which provides mechanistic insights into prior work that implicates these networks in a range of neuropsychiatric disorders.

Author contributions: A.C.C., D.J.O., G.H.G., K.D., and A.E. designed research; A.C.C., D.J.O., T.B., G.H.G., and A.E. performed research; A.C.C., D.J.O., C.C., Z.-W.Z., and A.E. analyzed data; and A.C.C., D.J.O., L.M.W., G.H.G., K.D., and A.E. wrote the paper.

The authors declare no conflict of interest.

This article is a PNAS Direct Submission.

[1]To whom correspondence may be addressed. E-mail: deissero@stanford.edu or amitetkin@stanford.edu.

This article contains supporting information online at www.pnas.org/lookup/suppl/doi:10.1073/pnas.1311772110/-/DCSupplemental.

SN, and DMN, not yet achieved, would not only carry fundamental implications for theoretical models of brain organization but also open up unique avenues for guiding neural network-modulating clinical interventions.

Causal effects were therefore operationalized in two ways with respect to testing whether and how the CEN and SN regulate the DMN: (*i*) that by exciting a putative CEN/SN regulatory node we induce DMN regulation, and (*ii*) that by inhibiting a putative CEN/SN regulatory node we perturb activity patterns in the DMN. Fig. 1 outlines the two sets of experiments that achieved these goals.

In the first set of experiments we used single excitatory TMS pulses, interleaved between acquisition of fMRI whole-brain volumes ("concurrent TMS/fMRI scans"), to separately drive nodes within the CEN or SN. We used psychophysiological interaction analyses (PPIs) as the read-out of the DMN's relationship with the CEN/SN and examined whether transient TMS-driven excitation of nodes within the CEN or SN induced the expected negative network relationship (Fig. 2 *A* and *B*). In the second set of experiments we acquired rs-fMRI scans before and after a single session of low-frequency (LF, 1 Hz) inhibitory repetitive TMS (rTMS) to CEN or SN nodes. We used analyses of resting-state signal amplitude and functional connectivity as read-outs of the downstream effects of rTMS on the DMN and examined whether 1-Hz rTMS-mediated inhibition of CEN or SN nodes resulted in disinhibition of DMN activity (Fig. 2*C*).

As such, our single-pulse TMS and rTMS experiments provided the external manipulation necessary for determining causality, whereas our DMN-focused fMRI analyses (PPI for single-pulse; signal amplitude and functional connectivity analyses for rTMS) measured the effects. Furthermore, on the basis of prior work, we expected that TMS excitation (single-pulse TMS/fMRI) and TMS inhibition (1-Hz rTMS) would produce effects in opposite directions. In motor cortex, for example, single-pulse TMS produces activation similar to voluntary engagement of this region (18), whereas inhibitory rTMS suppresses cortical excitability (e.g., ref. 19)—opposite direction effects, although not precisely opposite from a mechanistic perspective, given that single-pulse is an event-related activation tool as opposed to rTMS, which is meant to induce neuromodulation. Finally, as a secondary goal, we determined whether excitation or inhibition of nodes within the CEN or SN could also differentially modulate patterns of connectivity and/or signal amplitude within the CEN and SN.

Results

Two right-sided cortical nodes were selected as targets for TMS manipulations in this study for (*i*) constituting part of the CEN or SN, (*ii*) location in the prefrontal cortex, and (*iii*) accessibility to TMS modulation (Fig. 2*D* and Fig. S1). Thus, we selected a CEN node in the posterior middle frontal gyrus (pMFG) and an SN node in the anterior middle frontal gyrus (aMFG). These sites were mapped using an independent component analysis (ICA) on rs-fMRI scans from a separate dataset (n = 38) and subsequently transformed to individual subject native space for TMS targeting (Fig. S1). Consistent with prior work (12) and our TMS targeting approach, ICA based on all rs-fMRI scans from the experimental group (n = 22; including both pre- and post-rTMS scans) was used to define the canonical a priori regions of interest that best represent the three networks (Fig. 2*E* and Table S1): the right lateral prefrontal and lateral parietal cortices in the CEN, the dorsal anterior cingulate cortex (dACC) and the right fronto-insular complex (FIC) in the SN, and the medial prefrontal (MPFC) and posterior cingulate cortices (PCC) in the DMN. By having two active stimulation sites we were able to control for nonspecific effects of TMS stimulation (20), because believable sham stimulation is presently difficult to achieve in the MRI environment.

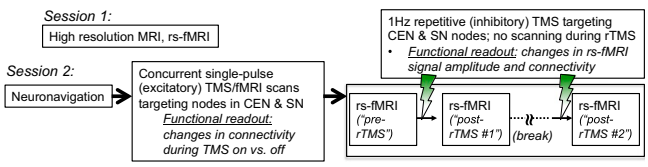

Fig. 1. Outline of the procedures in this study. The study consisted of two sessions occurring on separate days.

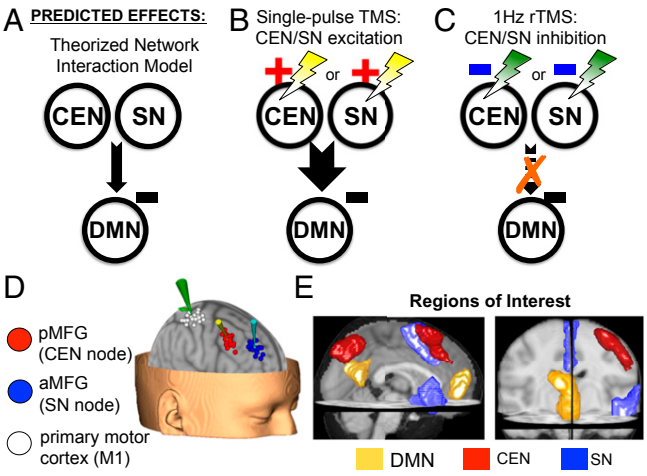

Fig. 2. (*A*) The theorized model for an inhibitory relationship between the DMN and CEN/SN. (*B*) Single-pulse TMS was used to excite CEN or SN nodes. (*C*) rTMS (1 Hz) was used to inhibit CEN or SN nodes. (*D*) TMS stimulation sites (determined using an ICA on rs-fMRI data from an independent set of healthy subjects) and primary motor cortex (M1) by subject. (*E*) Network a priori ROIs, defined using an ICA across all rs-fMRI scans in the experimental group.

Excitatory TMS/fMRI. To test our first causality prediction, we delivered excitatory single TMS pulses interleaved between acquisitions of whole-brain fMRI volumes to either the pMFG (CEN) or aMFG (SN). PPI analyses served as our neuroimaging read-out of the effects of single-pulse TMS and allowed us to quantitate TMS-induced connectivity between the DMN and CEN/SN. Our PPI "psychological context" was the short blocks during which interleaved TMS pulses were delivered, compared with no-TMS baseline periods (*Methods*). Results were analyzed in a 2 × 2 × 4 ANOVA with a two-level TMS stimulation target factor (i.e., pMFG and aMFG), a two-level PPI seed region factor (i.e., MPFC and PCC for the DMN), and a four-level PPI connectivity target factor (i.e., lateral prefrontal, lateral parietal, dACC, and FIC). We focused first on the main effect of TMS stimulation target, with subsequent dismantling of the ANOVA to identify specific effects (see also schematic summary in Fig. S2).

The overall 2 × 2 × 4 ANOVA (i.e., including all four CEN/SN regions as PPI connectivity targets) revealed a significant main effect of TMS stimulation target ($F_{1,21}$ = 6.1, P = 0.02), which was driven by greater induction of negative PPI connectivity between the DMN and the CEN/SN in response to pMFG (CEN), compared with aMFG (SN), excitatory single-pulse TMS (Fig. 3*A*). In fact, only pMFG stimulation induced negative DMN connectivity with the CEN/SN [vs. baseline: pMFG $t(21)$ = −3.4, P = 0.003; aMFG $t(21)$ = −0.4, P = 0.68]. The significant effect of TMS stimulation target also held when considering DMN connectivity with only the CEN in a 2 × 2 × 2 ANOVA ($F_{1,21}$ = 10.1, P = 0.005; Fig. 3*B*) and was furthermore significant in separate 2 × 2 ANOVAs for only DMN/lateral prefrontal PPI

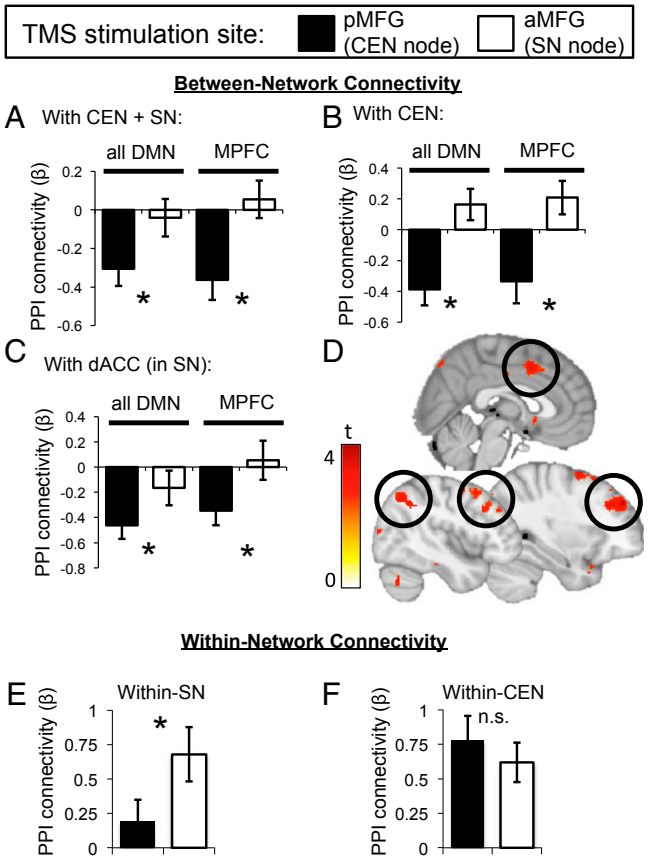

Fig. 3. TMS modulates network-level PPI connectivity. Single-pulse excitatory TMS to the pMFG (CEN node), but not to the aMFG (SN node), resulted in (*A*) negative DMN PPI connectivity with the combined CEN and SN, which was furthermore observed only for the MPFC node of the DMN, (*B*) negative DMN PPI connectivity with the CEN alone (also driven by the DMN's MPFC component), and (*C*) negative DMN PPI connectivity with only the dACC component of the SN (also driven by the DMN's MPFC component). (*D*) Illustrative voxelwise map of the MPFC-seeded PPI connectivity difference in response to pMFG (relative to aMFG) single-pulse TMS ($P < 0.005$, uncorrected). Positive signals indicate greater negative connectivity in response to single-pulse TMS to the pMFG. (*E*) Within-SN PPI connectivity is preferentially induced by aMFG stimulation, whereas (*F*) within-CEN PPI connectivity is induced by both stimulation sites.

connectivity ($F_{1,21} = 8.9$, $P = 0.007$) or only DMN/lateral parietal PPI connectivity ($F_{1,21} = 4.6$, $P = 0.045$).

When considering the main effect of TMS stimulation target for PPI connectivity between the DMN and only the SN, on the other hand, the 2 × 2 × 2 ANOVA for induced negative DMN PPI connectivity with the whole SN was not significant ($F_{1,21} = 1.2$, $P > 0.29$), although there was a significant interaction between the TMS stimulation target and PPI connectivity target within the SN (i.e., dACC vs. FIC; $F_{1,21} = 5.21$, $P = 0.031$). This latter interaction reflected significant induction of negative connectivity only in the DMN/dACC PPI in response to pMFG single-pulse TMS in a 2 × 2 ANOVA, which was absent with aMFG single-pulse TMS ($F_{1,21} = 4.2$, $P = 0.05$; Fig. 3*C*).

The 2 × 2 × 4 ANOVA also revealed a significant interaction between TMS stimulation target and DMN PPI seed region ($F_{1,21} = 4.2$, $P = 0.05$), which was driven by stronger induction of negative DMN connectivity (with the CEN and SN) for MPFC-seeded, compared with PCC-seeded, PPI analyses. For the MPFC DMN PPI seed alone, a 2 × 4 ANOVA examining the effects of TMS stimulation target and CEN/SN PPI connectivity target found a significant main effect of TMS stimulation target ($F_{1,21} = 11.9$, $P = 0.002$; Fig. 3*A*), whereas a similar analysis for PCC-seeded PPI connectivity did not ($F_{1,21} = 0.7$, $P > 0.43$).

This effect of TMS stimulation target for the MPFC PPI seed reflected greater induction of negative MPFC connectivity with the CEN in response to pMFG single-pulse TMS compared with aMFG TMS ($F_{1,21} = 13.3$, $P = 0.002$; Fig. 3*B*). In a similar fashion, MPFC also had greater negative connectivity with the dACC component of the SN after pMFG compared with aMFG stimulation [$t(21) = -2.3$, $P = 0.03$; Fig. 3*C*] but only at trend level for the entire SN ($F_{1,21} = 3.5$, $P = 0.074$), similar to what was seen for the combined DMN region analysis above. These effects are shown voxelwise in Fig. 3*D*, in which an MPFC-seeded PPI yields CEN and SN clusters.

These data indicate that (*i*) a causal inhibitory relationship exists between the CEN/SN and the DMN and that TMS stimulation of the pMFG node within CEN is sufficient to induce it, and (*ii*) that the greatest induction of negative DMN connectivity was between the MPFC component of the DMN and the lateral prefrontal, lateral parietal, and dACC regions of the CEN/SN. Importantly, CEN stimulation results in the expected negative PPI connectivity pattern, even when examining connectivity between the CEN's parietal cortex node and the MPFC (Fig. 3*D* and Fig. S3), thus illustrating that we have effectively driven brain network interactions and not just interactions between the stimulated brain area and downstream regions.

Finally, we examined *within*-CEN and *within*-SN effects of single-pulse TMS to examine whether excitation of nodes within the CEN or SN could also differentially modulate *within*-network connectivity. We found for the SN a significant effect of TMS stimulation target, such that aMFG stimulation enhanced within-SN PPI connectivity more than pMFG stimulation ($F_{1,21} = 5.49$, $P = 0.029$; Fig. 3*E*). This effect was driven by induction of positive within-SN PPI connectivity after aMFG stimulation [$t(21) = 3.44$, $P = 0.002$] but not after pMFG stimulation [$t(21) = 1.27$, $P = 0.22$]. By contrast, both stimulation sites induced similarly positive within-CEN PPI connectivity [$t(21) > 4.33$, $P < 0.001$; Fig. 3*F*). These data are consistent with prior work showing that single TMS pulses exert an excitatory effect on their targets (18) and thus serve as a "positive control."

Inhibitory rTMS with fMRI. To test our second causality prediction, we delivered 20-min trains of inhibitory 1-Hz rTMS to either the pMFG (CEN) or aMFG (SN) stimulation targets. We acquired resting-state fMRI scans before and after each train of rTMS to serve as the neuroimaging read-out of the after-effects of rTMS. We considered two resting-state metrics within the DMN, namely frequency-related signal amplitude and functional connectivity. Resting-state signal amplitude in the DMN is greatest in the 0.008- to 0.1-Hz LF range, although shifts to the immediately higher 0.1- to 0.25-Hz (high frequency, HF) range have been found for subjects in whom the DMN has become dysregulated (21). We therefore examined both LF (Fig. 4 *A* and *B*) and HF (Fig. 4 *C* and *D*) signal amplitude in the DMN as a function of inhibitory 1-Hz rTMS to the pMFG or aMFG.

With respect to signal amplitude, a 2 × 3 ANOVA with a two-level DMN region factor and three-level session factor (baseline, post-pMFG 1-Hz rTMS, post-aMFG 1-Hz rTMS) revealed a significant main effect of session ($F_{2,20} = 7.57$, $P = 0.004$). This reflected both a reduction of LF signal amplitude in the DMN after rTMS to either TMS node (Fig. 4*A*) and a significantly greater reduction in DMN LF signal amplitude after pMFG rTMS than after aMFG rTMS ($F_{1,21} = 7.02$, $P = 0.015$). There was also a significant main effect of DMN region ($F_{1,21} = 4.88$, $P = 0.038$). This was driven by a significant main effect of session for the MPFC ($F_{2,20} = 8.6$, $P = 0.002$; Fig. 4*A*) but no effect of session for the PCC ($F_{2,20} = 1.46$, $P = 0.26$). Within the MPFC, we observed a decrease in LF signal amplitude after rTMS to

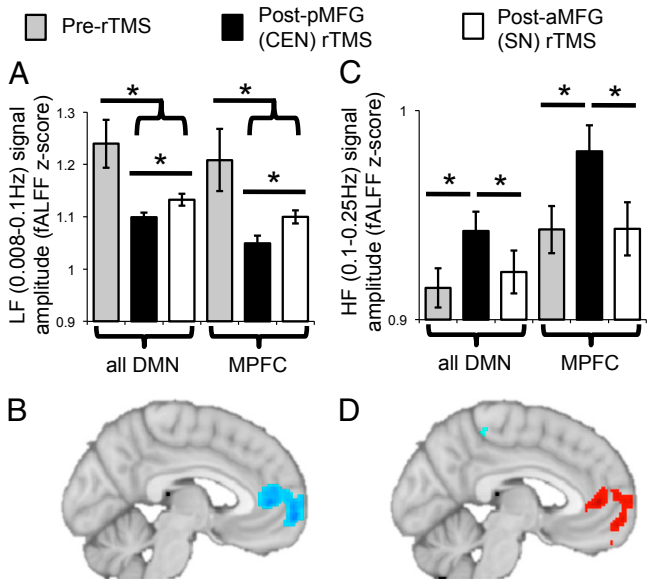

Fig. 4. Disinhibition of endogenous DMN activity after 1-Hz rTMS to the pMFG (CEN node), as reflected by (*A*) a shift of DMN signal, primarily in the MPFC (*B*), from lower frequencies (0.008–0.1 Hz) to (*C* and *D*) higher frequencies (0.1–0.25 Hz), plotted for the DMN (MPFC and PCC) or MPFC alone. The illustrative voxelwise maps show the difference in LF (*B*) or HF (*D*) signal amplitude for the difference between resting-state scans after 1-Hz pMFG rTMS compared with after 1-Hz aMFG rTMS ($P < 0.005$, uncorrected).

either TMS target, as well as a greater decrease in MPFC LF signal amplitude after pMFG rTMS than after aMFG rTMS ($F_{1,21} = 9.46$, $P = 0.006$). Fig. 4*B* illustrates these results at the voxelwise level.

As observed in other contexts (21), the reduction of DMN LF signal amplitude by pMFG rTMS was accompanied by a specific increase in DMN HF signal amplitude, consistent with disinhibition of the DMN (Fig. 4*C*). We observed a significant main effect of session for HF signal amplitude ($F_{2,20} = 5.51$, $P = 0.012$), which was driven by higher DMN HF signal amplitude after pMFG rTMS than either after aMFG rTMS ($F_{1,21} = 4.9$, $P = 0.038$) or at the pre-rTMS baseline ($F_{1,21} = 10.59$, $P = 0.004$). Similarly, there was a main effect of DMN region ($F_{1,21} = 38.34$, $P < 0.001$). This was driven by a significant main effect of session for the MPFC ($F_{2,20} = 6.08$, $P = 0.009$; Fig. 4*C*) and not for the PCC ($F_{2,20} = 1.36$, $P = 0.28$). Within the MPFC, we observed greater increases in HF signal amplitude after pMFG rTMS than either after aMFG rTMS ($F_{1,21} = 9.33$, $P = 0.006$) or at the pre-rTMS baseline ($F_{1,21} = 10.99$, $P = 0.003$). Fig. 4*D* qualitatively illustrates these a priori region of interest results at the voxelwise level. Outside of the DMN, rTMS to either the pMFG or aMFG similarly reduced LF signal amplitude in the SN and increased its HF signal amplitude (Fig. S4).

With respect to resting-state functional connectivity, we observed a significant main effect of session on LF range intra-DMN resting connectivity ($F_{2,20} = 4.57$, $P = 0.023$), such that intra-DMN resting connectivity was reduced after rTMS to either the pMFG or aMFG (Fig. S5). However, there was no difference in intra-DMN connectivity after pMFG compared with after aMFG rTMS ($F_{1,21} = 0.18$, $P = 0.67$). Together, these data suggest that there may be greater redundancy in determining connectivity patterns than amplitude of regional resting-state signal, such that inhibition of a single network node is enough to perturb regional signal amplitude but not connectivity. In summary, this loss-of-function experiment with inhibitory rTMS shows that endogenous CEN activity, as modulated through its pMFG node, is necessary for regulating the typical LF pattern of DMN signal, in particular for the MPFC, without which the DMN's activity becomes disinhibited, shifting its signal from lower to higher frequency.

Stimulation Locations Relative to Motor Cortex. Finally, we explored the relationship between our connectivity-guided TMS stimulation targets and the current standard clinical procedure for targeting of rTMS for depression [i.e., "the 5- or 6-cm rule"; (22–26)]. At present, this is the only US Food and Drug Administration-approved brain rTMS-based treatment for any clinical indication and involves stimulation aimed at the dorsolateral prefrontal cortex, at a site 5–6 cm anterior to the primary motor cortex (M1). We therefore mapped M1 in our subjects, guided by the hand knob landmark (27) and confirmed by evoking motor responses from the contralateral abductor pollicis brevis muscle, and compared the distance from M1 to the pMFG and aMFG stimulation sites in each subject. There were two distinct clusters corresponding to the pMFG and aMFG stimulation targets, which were 3.4 ± 0.1 cm apart (Fig. 2*D*). The mean distance from M1 to the pMFG site was 5.4 ± 0.2 cm and from M1 to the aMFG site was 8.4 ± 0.2 cm. There is therefore a remarkably close parallel between the 5- or 6-cm rule that has been adopted clinically and our connectivity-guided pMFG target in the CEN.

Discussion

Here we directly tested a long-standing assumption based on correlations, that the CEN and SN exert control over the DMN, a notion that has been theorized but never proven in terms of causality (9, 10, 12, 28, 29). In so doing, our TMS/fMRI findings demonstrate a directional causal relationship by which a dorsolateral prefrontal node situated within the CEN inhibits CEN interactions primarily with the MPFC portion of the DMN. Connectivity analyses typically find similar CEN/SN connectivity relationships for both PCC and MPFC (2, 9) (although also see ref. 30) and cannot definitively discriminate as to their causal origin. It is only through external manipulation of brain activity, accomplished here by single-pulse excitatory TMS and inhibitory rTMS, that specific causal pathways in the brain can be identified. Moreover, although we cannot rule out that an as-yet-unidentified third region mediates the effect of dorsolateral prefrontal on the MPFC, our results indicate a causal chain between manipulation of the dorsolateral prefrontal cortex and effects on the MPFC. This is further supported by evidence of a monosynaptic projection between these structures (31).

It is also noteworthy that resting DMN activity was altered after inhibitory rTMS to a regulatory node in the CEN. Thus, even in the absence of CEN engagement by a task, activity in the CEN is important for maintaining the typical LF pattern of DMN signal. Indeed, the CEN is active even when subjects are at rest (32) and when active would presumably lead to transient inhibition of DMN activity. The specific ways in which the CEN and DMN interact under physiological conditions, however, is not yet fully clear. Finally, alterations in the resting-state relationship between the CEN/SN and DMN are seen in particular behavioral states in the same individual, as well as differ between healthy individuals and those with psychopathology. Hence, the resting-state relationship between the CEN/SN and DMN is modifiable (in our case by rTMS) (6, 33). One caveat is that we did not find an effect on the CEN of dorsolateral prefrontal rTMS, and thus interpret the inhibitory effect of 1-Hz rTMS on the basis of extensive prior data (34). Interestingly, the effects on downstream targets (DMN) but not within-network targets in the CEN are also consistent with our recently completed study of depression treatment with rTMS (10 Hz) to the left dorsolateral prefrontal cortex, in which we found changes after treatment in the DMN but not within the CEN.

During attention-demanding tasks, activation is frequently observed in the human CEN and SN using either functional

neuroimaging or intracranial electrophysiological measures, whereas deactivation is observed within the DMN (28, 35). Similar effects have been observed in both cats and monkeys (36, 37). As such, dynamic opposition between activation of the CEN/SN and deactivation of the DMN has been theorized to mediate transitions between rest and task-engaged states (2, 4, 6, 7, 9, 10). Disruptions in this dynamic opposition between networks have been linked to attentional lapses and suboptimal performance in healthy subjects (38–41). Thus, because the CEN has been proposed to play a preferential role in trial-to-trial adaptive control (5), such adaptation may involve balancing internally oriented DMN activity and externally oriented task-related CEN/SN activity (6). These hypotheses with regard to consequences of pMFG (i.e., CEN) excitatory or inhibitory rTMS on task-related processing can be tested directly in future work examining the effects of HF and LF rTMS on task performance and activation.

Although we do not rule out the possibility that other SN sites may regulate the DMN (12), we provided strong evidence that stimulating the most TMS-accessible SN node (aMFG) increased within-SN PPI connectivity, while still leaving SN/DMN PPI connectivity unaffected. It will be important to extend this study by investigating other targets [e.g., right FIC (12)], left-sided network nodes, contrast the effects of inhibitory LF and excitatory HF rTMS, as well as stimulate the MPFC component of the DMN directly and examine effects on the CEN/SN (although deeper sites are difficult to reach with conventional TMS coils). Additionally, it would be of interest to apply mathematical modeling methods previously used to examine network relationships (12) to our post-rTMS resting-state data. One notable limitation of our study that could be remedied in future work is the lack of a sham rTMS condition. Presence of a sham condition would have allowed us to interpret effects common to pMFG and aMFG rTMS (e.g., Figs. S4 and S5) but was not feasible in the context of the present study. Nonetheless, having two distinct active targets for TMS in this study allowed one to serve as a control for the other.

Identification of a node in the CEN that regulates the DMN also carries clinical implications. The DMN shows various abnormalities in a range of neuropsychiatric disorders, including depression, posttraumatic stress disorder, schizophrenia, Alzheimer's disease, and autism (13, 14, 33, 42). We also note in particular that the MPFC, which is one key part of the DMN, has been postulated to be critical for the antidepressant effects of medications and rTMS (43, 44). The clinical efficacy of rTMS, however, remains fairly limited, owing to a poor mechanistic understanding of the effects of rTMS and suboptimal targeting of stimulation, which currently makes minimal explicit reference to patients' structural or functional neuroanatomy (44, 45). It is therefore intriguing that the MPFC-regulating CEN node (pMFG) was located 5–6 cm anterior of primary motor cortex, consistent with current methods for localizing the clinical rTMS stimulation site (25, 26). Thus, because connectivity-guided modulation of this node selectively regulates the MPFC/DMN, our results may serve as a unique platform for circuit-driven interventions in humans, including for depression.

Methods

Subjects. The TMS/fMRI study included 24 healthy subjects (age 26.5 ± 0.9 y, 14 males). Two participants were excluded from the TMS/fMRI data analysis because they failed to complete the study. Scan parameters and preprocessing are described in *SI Methods*.

TMS Targeting. TMS targets were identified using a frameless stereotactic neuronavigation system (Brainsight2; Rogue Research) on rs-fMRI ICA maps (http://www.fmrib.ox.ac.uk/fsl/melodic/index.html) from a separate cohort of 38 healthy subjects (Fig. S1). Stimulation spots were marked on a Lycra swim cap (Speedo USA) worn by the subject inside the scanner (45), consistent with prior TMS/fMRI studies (18). TMS was delivered by a MagStim 70-mm figure-eight MR-compatible coil inside the MRI machine, held in place with a custom-built MRI coil holder, and controlled by a MagStim Rapid2 stimulator located outside the scanner room and connected to the coil through the penetration panel. Noise in the functional images otherwise induced by the MagStim system was eliminated through custom implementation of radio frequency filters at the penetration panel. The TMS coil was repositioned for each stimulation site by sliding the subject out of the scanner bore, adjusting the coil holder position, returning the subject into the scanner bore, and retaking anatomic calibration scans. Stimulation intensity was individually determined and delivered at 120% of each subject's resting motor threshold. We also recorded subjective discomfort ratings at baseline, as well as immediately after each experimental TMS manipulation (Subjective Units of Distress Scale).

Interleaved Single-Pulse TMS/fMRI. At each stimulation site, 70 TMS pulses were delivered over 5 min (147 volumes) in a miniblock design with 7 pulses per block and 10 blocks per run. Pulses were delivered between functional volumes to avoid corruption of blood oxygen level-dependent signal (17), resulting in a stimulation frequency of 0.4 Hz during each 16.8-s "TMS on" period (which were separated from each other by 16.8-s "TMS off" no-stimulation periods). Prior work has not found effects of single-pulse TMS delivered in this way on cortical excitability when stimulation is slower than 0.9 Hz (19), and has found that a single-pulse interleaved TMS/fMRI protocol similar to ours does not induce lasting plasticity that would affect subsequent scans (46).

rTMS and Resting-State Scans. In session 1 we collected one 8-min (240 volumes) eyes-open resting-state fMRI scan, and in session 2 we collected three 8-min scans, one before any rTMS, and two that immediately followed rTMS to the CEN or SN nodes. For each stimulation site, a 20-min train of 1-Hz rTMS (1,200 pulses) was delivered while subjects were inside the scanner. rTMS epochs were separated by 35–40 min to ensure signal/physiological recovery. Low frequency (~1 Hz) rTMS, when applied over motor cortex or visual cortex, leads to suppressed local cortical excitability that lasts for approximately the same duration as the rTMS after the end of stimulation, as indexed by decreased motor-evoked potentials (47), increased phosphene threshold (48), or on EEG measures of cortical excitability (34). Finally, the order of sites receiving 1-Hz rTMS was counterbalanced across subjects.

Network Definition for Analyses. A priori network regions of interest (ROIs) consistent with the specific nature of our hypotheses were defined by ICA across the experimental group, including both pre- and post-rTMS scans. Following prior work (12), two key regions were identified for each of the networks. As shown in Fig. 2*E* and Table S1, the resulting six ROIs included the ~1,000 highest functionally connected voxels (~8,000 mm^3) and encompassed the DMN (MPFC, PCC), CEN (right-sided lateral prefrontal, lateral parietal cortices), and SN (dACC, right FIC). We focused on ROI-based extractions from the right hemisphere because (*i*) the CEN in particular is highly lateralized (e.g., ICA map in Fig. S1*A*), and (*ii*) network dynamics between the DMN, CEN, and SN have been shown to be more robust in the right hemisphere (12).

Analysis of Concurrent TMS/fMRI Data. To examine the effects of single-pulse TMS on network interactions, we used PPI [SPM8 (http://www.fil.ion.ucl.ac.uk/spm)], which tests whether interregional correlations ("functional connectivity") change as a function of the intermittent TMS stimulations, while accounting for mean activity changes due to the main effect of stimulation (49). Briefly, to create the PPI interaction term of interest, signal in a seed ROI is deconvolved (50), multiplied with a vector coding for when TMS stimulation occurred, then reconvolved with the hemodynamic response function, and finally entered into a model containing the seed ROI time series and TMS stimulation vector. Thus, our "psychological term" in the PPI was the "TMS on" periods, which correspond to when short blocks of interleaved single TMS pulses were delivered, separated by baseline ("TMS off") no-stimulation periods. This approach is consistent with our own previous publications using PPI (51) and the use of "generalized PPI" methods (52).

Analysis of Resting-State Data—Signal Amplitude. We used a fractional amplitude of LF fluctuations analysis (fALFF; http://www.restfmri.net/) (53), which measures the amplitude of regional signal in a frequency range relative to the signal from the whole detectable frequency spectrum. rs-fMRI data were transformed into the frequency domain with a Fast Fourier transform and then square-rooted to obtain the amplitude. fALFF was calculated as the sum of amplitudes across the ranges of 0.008–0.1 Hz (LF) (54) or 0.1–0.25 Hz (HF), divided by the signal across the entire frequency range, and standardized by *z* transformation, which improves statistical analyses and test–retest reliability (55).

Analysis of Resting-State Data—Connectivity. Band-pass filtered resting-state data were analyzed for connectivity between regions by performing correlations between the time courses of each pair of regions within a network. These *r* values were then *z*-transformed for statistical analyses.

Statistical Analyses. All statistical analyses were conducted using SPSS 18. The specifics of each ANOVA and *t* test performed are detailed in *Results*. All error bars represent SEM.

ACKNOWLEDGMENTS. We thank Anett Gyurak, Alan Schatzberg, and Paul Hamilton for comments on the manuscript. A.E. was supported by National Institutes of Health (NIH) Grants P30 MH089888 and R01 MH091860, and the Sierra-Pacific Mental Illness Research Education and Clinical Center at the Palo Alto Department of Veterans Affairs (VA). K.D. was supported by the NIH, the Wiegers Family Fund, and the Snyder Foundation. G.H.G. was supported by NIH Grant P41 EB015891. D.J.O. was supported by the War Related Illness and Injury Study Center Special Fellowship Program at the VA Palo Alto and the Medical Research Service of the Department of Veterans Affairs, VA Palo Alto.

1. Becerra L, Pendse G, Chang PC, Bishop J, Borsook D (2011) Robust reproducible resting state networks in the awake rodent brain. *PLoS One* 6(10):e25701.
2. Raichle ME (2011) The restless brain. *Brain Connect* 1(1):3–12.
3. Power JD, et al. (2011) Functional network organization of the human brain. *Neuron* 72(4):665–678.
4. Deco G, Jirsa VK, McIntosh AR (2011) Emerging concepts for the dynamical organization of resting-state activity in the brain. *Nat Rev Neurosci* 12(1):43–56.
5. Dosenbach NU, Fair DA, Cohen AL, Schlaggar BL, Petersen SE (2008) A dual-networks architecture of top-down control. *Trends Cogn Sci* 12(3):99–105.
6. Sonuga-Barke EJ, Castellanos FX (2007) Spontaneous attentional fluctuations in impaired states and pathological conditions: A neurobiological hypothesis. *Neurosci Biobehav Rev* 31(7):977–986.
7. Anticevic A, et al. (2012) The role of default network deactivation in cognition and disease. *Trends Cogn Sci* 16(12):584–592.
8. Dosenbach NU, et al. (2007) Distinct brain networks for adaptive and stable task control in humans. *Proc Natl Acad Sci USA* 104(26):11073–11078.
9. Fox MD, et al. (2005) The human brain is intrinsically organized into dynamic, anticorrelated functional networks. *Proc Natl Acad Sci USA* 102(27):9673–9678.
10. Fransson P (2005) Spontaneous low-frequency BOLD signal fluctuations: An fMRI investigation of the resting-state default mode of brain function hypothesis. *Hum Brain Mapp* 26(1):15–29.
11. Murphy K, Birn RM, Handwerker DA, Jones TB, Bandettini PA (2009) The impact of global signal regression on resting state correlations: Are anti-correlated networks introduced? *Neuroimage* 44(3):893–905.
12. Sridharan D, Levitin DJ, Menon V (2008) A critical role for the right fronto-insular cortex in switching between central-executive and default-mode networks. *Proc Natl Acad Sci USA* 105(34):12569–12574.
13. Buckner RL, Andrews-Hanna JR, Schacter DL (2008) The brain's default network: Anatomy, function, and relevance to disease. *Ann N Y Acad Sci* 1124:1–38.
14. Menon V (2011) Large-scale brain networks and psychopathology: A unifying triple network model. *Trends Cogn Sci* 15(10):483–506.
15. Driver J, Blankenburg F, Bestmann S, Vanduffel W, Ruff CC (2009) Concurrent brain-stimulation and neuroimaging for studies of cognition. *Trends Cogn Sci* 13(7):319–327.
16. Siebner HR, et al. (2009) Consensus paper: Combining transcranial stimulation with neuroimaging. *Brain Stimulat* 2(2):58–80.
17. Bohning DE, et al. (1998) Echoplanar BOLD fMRI of brain activation induced by concurrent transcranial magnetic stimulation. *Invest Radiol* 33(6):336–340.
18. Denslow S, Lomarev M, Bohning DE, Mu Q, George MS (2004) A high resolution assessment of the repeatability of relative location and intensity of transcranial magnetic stimulation-induced and volitionally induced blood oxygen level-dependent response in the motor cortex. *Cogn Behav Neurol* 17(3):163–173.
19. Fitzgerald PB, Fountain S, Daskalakis ZJ (2006) A comprehensive review of the effects of rTMS on motor cortical excitability and inhibition. *Clin Neurophysiol* 117(12):2584–2596.
20. Fox MD, Halko MA, Eldaief MC, Pascual-Leone A (2012) Measuring and manipulating brain connectivity with resting state functional connectivity magnetic resonance imaging (fcMRI) and transcranial magnetic stimulation (TMS). *Neuroimage* 62(4):2232–2243.
21. Baliki MN, Baria AT, Apkarian AV (2011) The cortical rhythms of chronic back pain. *J Neurosci* 31(39):13981–13990.
22. Pascual-Leone A, Rubio B, Pallardó F, Catalá MD (1996) Rapid-rate transcranial magnetic stimulation of left dorsolateral prefrontal cortex in drug-resistant depression. *Lancet* 348(9022):233–237.
23. George MS, et al. (1995) Daily repetitive transcranial magnetic stimulation (rTMS) improves mood in depression. *Neuroreport* 6(14):1853–1856.
24. George MS, et al. (1996) Changes in mood and hormone levels after rapid-rate transcranial magnetic stimulation (rTMS) of the prefrontal cortex. *J Neuropsychiatry Clin Neurosci* 8(2):172–180.
25. George MS, et al. (2010) Daily left prefrontal transcranial magnetic stimulation therapy for major depressive disorder: A sham-controlled randomized trial. *Arch Gen Psychiatry* 67(5):507–516.
26. O'Reardon JP, et al. (2007) Efficacy and safety of transcranial magnetic stimulation in the acute treatment of major depression: A multisite randomized controlled trial. *Biol Psychiatry* 62(11):1208–1216.
27. Yousry TA, et al. (1997) Localization of the motor hand area to a knob on the precentral gyrus. A new landmark. *Brain* 120(Pt 1):141–157.
28. McKiernan KA, Kaufman JN, Kucera-Thompson J, Binder JR (2003) A parametric manipulation of factors affecting task-induced deactivation in functional neuroimaging. *J Cogn Neurosci* 15(3):394–408.
29. Northoff G, et al. (2007) GABA concentrations in the human anterior cingulate cortex predict negative BOLD responses in fMRI. *Nat Neurosci* 10(12):1515–1517.
30. Uddin LQ, Kelly AM, Biswal BB, Castellanos FX, Milham MP (2009) Functional connectivity of default mode network components: Correlation, anticorrelation, and causality. *Hum Brain Mapp* 30(2):625–637.
31. Selemon LD, Goldman-Rakic PS (1988) Common cortical and subcortical targets of the dorsolateral prefrontal and posterior parietal cortices in the rhesus monkey: Evidence for a distributed neural network subserving spatially guided behavior. *J Neurosci* 8(11):4049–4068.
32. Mantini D, Perrucci MG, Del Gratta C, Romani GL, Corbetta M (2007) Electrophysiological signatures of resting state networks in the human brain. *Proc Natl Acad Sci USA* 104(32):13170–13175.
33. Zhang D, Raichle ME (2010) Disease and the brain's dark energy. *Nat Rev Neurol* 6(1):15–28.
34. Thut G, Pascual-Leone A (2010) A review of combined TMS-EEG studies to characterize lasting effects of repetitive TMS and assess their usefulness in cognitive and clinical neuroscience. *Brain Topogr* 22(4):219–232.
35. Ossandón T, et al. (2011) Transient suppression of broadband gamma power in the default-mode network is correlated with task complexity and subject performance. *J Neurosci* 31(41):14521–14530.
36. Popa D, Popescu AT, Paré D (2009) Contrasting activity profile of two distributed cortical networks as a function of attentional demands. *J Neurosci* 29(4):1191–1201.
37. Mantini D, et al. (2011) Default mode of brain function in monkeys. *J Neurosci* 31(36): 12954–12962.
38. Weissman DH, Roberts KC, Visscher KM, Woldorff MG (2006) The neural bases of momentary lapses in attention. *Nat Neurosci* 9(7):971–978.
39. Prado J, Weissman DH (2011) Heightened interactions between a key default-mode region and a key task-positive region are linked to suboptimal current performance but to enhanced future performance. *Neuroimage* 56(4):2276–2282.
40. Eichele T, et al. (2008) Prediction of human errors by maladaptive changes in event-related brain networks. *Proc Natl Acad Sci USA* 105(16):6173–6178.
41. Persson J, Lustig C, Nelson JK, Reuter-Lorenz PA (2007) Age differences in deactivation: A link to cognitive control? *J Cogn Neurosci* 19(6):1021–1032.
42. Whitfield-Gabrieli S, Ford JM (2012) Default mode network activity and connectivity in psychopathology. *Annu Rev Clin Psychol* 8:49–76.
43. Pizzagalli DA (2011) Frontocingulate dysfunction in depression: Toward biomarkers of treatment response. *Neuropsychopharmacology* 36(1):183–206.
44. Fox MD, Buckner RL, White MP, Greicius MD, Pascual-Leone A (2012) Efficacy of transcranial magnetic stimulation targets for depression is related to intrinsic functional connectivity with the subgenual cingulate. *Biol Psychiatry* 72(7):595–603.
45. Herbsman T, et al. (2009) More lateral and anterior prefrontal coil location is associated with better repetitive transcranial magnetic stimulation antidepressant response. *Biol Psychiatry* 66(5):509–515.
46. Bohning DE, et al. (2000) BOLD-f MRI response to single-pulse transcranial magnetic stimulation (TMS). *J Magn Reson Imaging* 11(6):569–574.
47. Chen R, et al. (1997) Depression of motor cortex excitability by low-frequency transcranial magnetic stimulation. *Neurology* 48(5):1398–1403.
48. Boroojerdi B, Prager A, Muellbacher W, Cohen LG (2000) Reduction of human visual cortex excitability using 1-Hz transcranial magnetic stimulation. *Neurology* 54(7):1529–1531.
49. Friston KJ, et al. (1997) Psychophysiological and modulatory interactions in neuroimaging. *Neuroimage* 6(3):218–229.
50. Gitelman DR, Penny WD, Ashburner J, Friston KJ (2003) Modeling regional and psychophysiologic interactions in fMRI: The importance of hemodynamic deconvolution. *Neuroimage* 19(1):200–207.
51. Etkin A, Egner T, Peraza DM, Kandel ER, Hirsch J (2006) Resolving emotional conflict: A role for the rostral anterior cingulate cortex in modulating activity in the amygdala. *Neuron* 51(6):871–882.
52. McLaren DG, Ries ML, Xu G, Johnson SC (2012) A generalized form of context-dependent psychophysiological interactions (gPPI): A comparison to standard approaches. *Neuroimage* 61(4):1277–1286.
53. Zou QH, et al. (2008) An improved approach to detection of amplitude of low-frequency fluctuation (ALFF) for resting-state fMRI: Fractional ALFF. *J Neurosci Methods* 172(1):137–141.
54. Cordes D, et al. (2001) Frequencies contributing to functional connectivity in the cerebral cortex in "resting-state" data. *AJNR Am J Neuroradiol* 22(7):1326–1333.
55. Zuo XN, et al. (2010) The oscillating brain: Complex and reliable. *Neuroimage* 49(2): 1432–1445.

Supporting Information

Chen et al. 10.1073/pnas.1311772110

SI Results

Repetitive Transcranial Magnetic Stimulation Results—Reliability-Related Analyses. We examined the influence of two potential confounding factors with regard to the effects of repetitive transcranial magnetic stimulation (rTMS). When we included a between-subject experiment "sequence" factor [i.e., posterior middle frontal gyrus (pMFG) rTMS first vs. anterior MFG (aMFG) rTMS first] in the ANOVAs above, there was no significant session × sequence interaction for either of our key signal amplitude measures [low-frequency (LF) signal amplitude: $F_{2,19} = 1.56$, $P > 0.24$; high-frequency (HF) signal amplitude: $F_{2,19} = 0.64$, $P > 0.54$], whereas the main effect of session persisted (LF signal amplitude: $F_{2,19} = 7.3$, $P = 0.004$; HF signal amplitude: $F_{2,19} = 5.59$, $P > 0.012$). Thus, our counterbalancing procedure worked as intended. Next, we examined whether the observed LF and HF signal amplitude alterations with pMFG rTMS reflects a change greater than variation between repeated resting-state scans. Consistent with prior findings on the reliability of default mode network (DMN) resting signal (1), if we used the "session 1" resting scan in place of the pre-rTMS baseline resting scan, we found similarly significant effects of session for LF ($F_{2,20} = 17.73$, $P < 0.001$) and HF ($F_{2,20} = 4.8$, $P = 0.02$) signal amplitudes as reported above.

SI Methods

Structural MRI. A high-resolution T1-weighted spoiled grass gradient recalled inversion recovery 3D MRI sequence was used: inversion time (TI) = 400 ms, repetition time (TR) = 6.2 ms; echo time (TE) = 2 ms; flip angle = 15°; 25.6-cm field of view; 146 coronal slices (1.2-mm slice thickness); 256 × 256 matrix.

General Scan Parameters. We used a 1.5T GE Signa Excite scanner at Stanford University. Twenty-nine axial slices (4 mm thick) covered the whole brain, using a T2-weighted gradient-echo spiral-in/out pulse sequence (TE = 40 ms; flip angle = 85°; 22-cm field of view; 64 × 64 matrix, and one interleave; TR = 2,000 ms) (2). Resting-state scans were acquired with no pause between volumes, whereas concurrent TMS/fMRI scans were acquired with a 400-ms pause between volumes to allow interleaving of single TMS pulses (3). An automated high-order shimming method based on spiral acquisitions was used before acquiring fMRI scans (4).

fMRI Data Preprocessing. A linear shim correction was applied separately for each slice during reconstruction using a magnetic field map acquired automatically by the pulse sequence at the beginning of the scan (5). Preprocessing using FSL (http://www.fmrib.ox.ac.uk/fsl/) (6) included realignment, 6-mm FWHM Gaussian kernel smoothing, removal of linear temporal trends, and correction for physiological noise using measures of heart rate and respiration (7, 8). For resting-state scans, motion parameters and white matter/cerebrospinal fluid time courses were also regressed out. High-resolution structural scans were normalized to standard MNI space using a nonlinear high-resolution warp normalization method (FNIRT) to the matching Montreal Neurological Institute (MNI) 152 brain template (6).

We followed standard preprocessing methods. No participants had movement greater than 3 mm of translation or 3° of rotation. We also ruled out that differences in head motion (9, 10) or physical sensation during TMS to different sites confounded our findings, by calculating the maximum peak-to-peak excursion and rms fluctuation for all six motion parameters during resting-state scans and quantifying self-reported discomfort, and found no differences between stimulation targets across scans (all $P > 0.23$).

1. Van Dijk KR, et al. (2010) Intrinsic functional connectivity as a tool for human connectomics: Theory, properties, and optimization. *J Neurophysiol* 103(1): 297–321.
2. Glover GH, Law CS (2001) Spiral-in/out BOLD fMRI for increased SNR and reduced susceptibility artifacts. *Magn Reson Med* 46(3):515–522.
3. Bohning DE, et al. (1998) Echoplanar BOLD fMRI of brain activation induced by concurrent transcranial magnetic stimulation. *Invest Radiol* 33(6):336–340.
4. Kim DH, Adalsteinsson E, Glover GH, Spielman DM (2002) Regularized higher-order in vivo shimming. *Magn Reson Med* 48(4):715–722.
5. Glover GH, Lai S (1998) Self-navigated spiral fMRI: Interleaved versus single-shot. *Magn Reson Med* 39(3):361–368.
6. Jenkinson M, Beckmann CF, Behrens TE, Woolrich MW, Smith SM (2012) Fsl. *Neuroimage* 62(2):782–790.
7. Glover GH, Li TQ, Ress D (2000) Image-based method for retrospective correction of physiological motion effects in fMRI: RETROICOR. *Magn Reson Med* 44(1):162–167.
8. Chang C, Glover GH (2009) Effects of model-based physiological noise correction on default mode network anti-correlations and correlations. *Neuroimage* 47(4):1448–1459.
9. Van Dijk KR, Sabuncu MR, Buckner RL (2012) The influence of head motion on intrinsic functional connectivity MRI. *Neuroimage* 59(1):431–438.
10. Power JD, Barnes KA, Snyder AZ, Schlaggar BL, Petersen SE (2012) Spurious but systematic correlations in functional connectivity MRI networks arise from subject motion. *Neuroimage* 59(3):2142–2154.

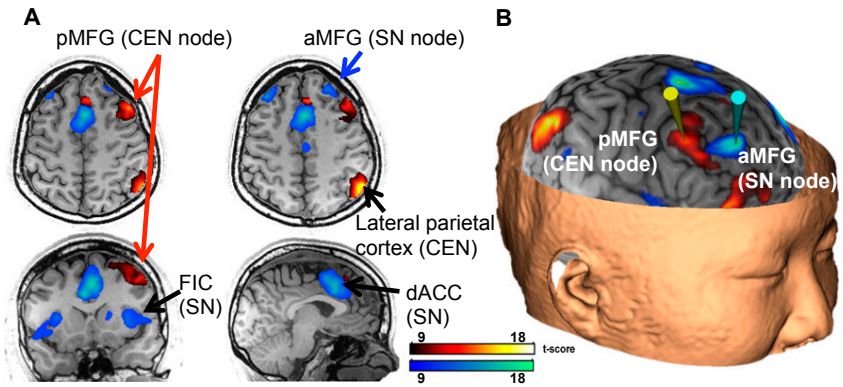

Fig. S1. Identification of stimulation sites for an individual subject. (*A*) Independent component analysis (ICA)-identified networks from a separate healthy subject cohort ($n = 38$) were used to map the fronto-parietal central executive network (CEN) (warm-color spectrum) and cingulo-opercular salience network (SN) (cool-color spectrum). Maps of these networks were reverse-normalized into each subject's native anatomical space and coregistered to their head using frameless stereotactic neuronavigation. The pMFG node of the CEN is indicated with red arrows, whereas the aMFG node of the SN is indicated with a blue arrow. Also shown are the parietal portion of the CEN and the dorsal anterior cingulate (dACC) and fronto-insular cortical (FIC) portions of the SN. (*B*) Example stimulation sites in native subject space, along with stimulation trajectories estimated to be perpendicular to the local orientation of the gyrus, were then selected according to the peak of ICA connectivity within the respective cluster: pMFG (yellow cone), aMFG (cyan cone).

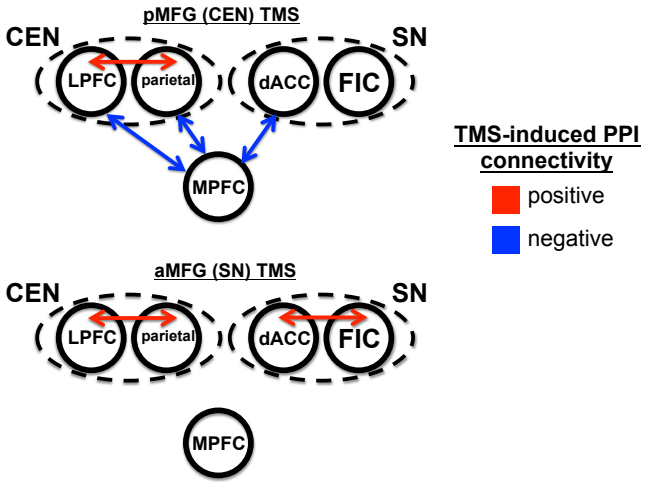

Fig. S2. Schematic diagram of the single-pulse TMS-induced psychophysiological interaction analysis (PPI) results observed in this study, between regions within the CEN [lateral prefrontal (LPFC), parietal], the SN (dACC, FIC), and the medial prefrontal cortex (MPFC) component of the DMN.

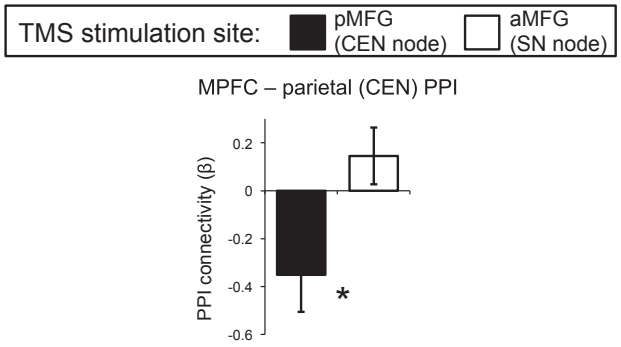

Fig. S3. Single-pulse excitatory TMS to the pMFG (CEN node), but not to the aMFG (SN node), resulted in negative PPI connectivity between the parietal node of the CEN and MPFC node of the DMN.

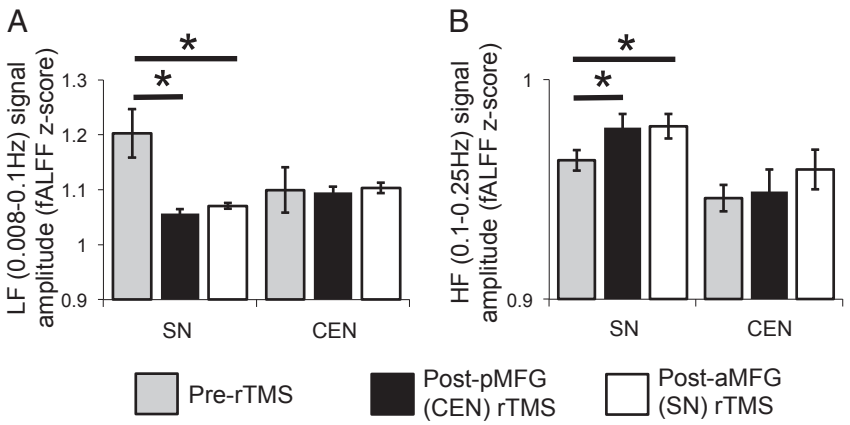

Fig. S4. No significant differences between effects of pMFG or aMFG rTMS were found for resting-state signal amplitude within the CEN or SN, although rTMS to either target led to decreased LF (*A*) and increased HF signal amplitude (*B*) in the SN.

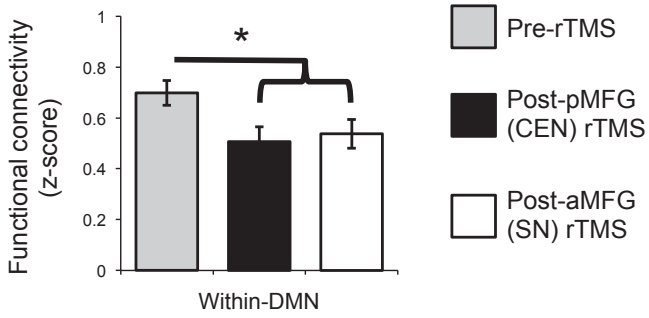

Fig. S5. No significant differences between effects of pMFG or aMFG rTMS were found for resting-state DMN functional connectivity, although rTMS to either target led to decreased connectivity in the DMN.

Table S1. Network a priori regions of interest

Region of interest	No. of voxels (mm^3)	Center-of-mass MNI coordinates (x, y, z)	Brodmann's area (BA)
MPFC	999 (7,992)	(−2, 53, 5)	9/10/11/32
Posterior cingulate cortex	1,006 (8,048)	(−1, −61, 16)	23/29/30/31
dACC	999 (7,992)	(1, 9, 52)	24/32/6
FIC	996 (7,968)	(49, 13, −6)	13/44/45/47
LPFC	994 (7,952)	(38, 16, 50)	6/8/9/46
Lateral parietal cortex	1,009 (8,072)	(45, −64, 40)	7/39/40